Eur. Phys. J. D (2018) 72: 84
https://doi.org/10.1140/epjd/e2018-80385-7

THE EUROPEAN PHYSICAL JOURNAL D

Regular Article

Recent progress in the theory and simulation of strongly correlated plasmas: phase transitions, transport, quantum, and magnetic field effects*

Torben Ott[a], Hauke Thomsen, Jan Willem Abraham, Tobias Dornheim, and Michael Bonitz

Christian-Albrechts-Universität Kiel, Institut für Theoretische Physik and Astrophysik, Leibnizstraße 15, 24098 Kiel, Germany

Received 7 June 2017 / Received in final form 15 October 2017
Published online 22 May 2018 – © EDP Sciences, Società Italiana di Fisica, Springer-Verlag 2018

Abstract. We review recent progress in theory and simulation of strongly correlated classical plasmas, in general, and dusty plasmas, in particular. Using the one-component plasma (OCP) as a model, the structural properties of extended and finite correlated systems are analyzed and criteria for disordering transitions are introduced. These are based on the pair and three-particle distribution functions and the associated reduced entropies and heat capacities. These quantities are computed from the particle positions alone and are, thus, directly accessible in experiments. Further, these quantities are applied to confined systems where disordering proceeds via a sequence of phase transitions which have to be clearly distinguished. In the second part of this review, the transport properties of strongly correlated plasmas in equilibrium are considered, particularly under the influence of an external magnetic field. Examples given are for the diffusion, heat conduction and viscosity. Here, the influence on both fundamental transport coefficients and on particle-resolved dynamical effects is considered. Finally, we give a brief discussion of spin and quantum effects and how they influence the structural and dynamical properties of correlated systems.

1 Introduction

Strongly correlated systems are ubiquitous. They are observed in a variety of fields – from ultracold plasmas [1], cold atoms in optical lattices [2], dusty plasmas [3] and inertial confinement fusion [4] to the physics of planet interiors [5] and neutron stars [6,7]. The theoretical description of strongly correlated systems in general and plasmas, in particular, is challenging because they lack – unlike weakly coupled or crystalline systems – a single small parameter around which an analytical solution can be expanded. Thus, these systems are a fertile ground for the development of theoretical models, simulations, and numerical approaches.

In this review paper, we focus on the progress made in computationally and theoretically describing the structural properties, particularly phase transitions, and the transport properties of dusty plasmas and one-component plasmas in the German Transregional Research Center TRR24 "Fundamentals of Complex Plasmas" in the recent five years [8–41] and put this into the context of other modern developments. Another objective is to compare correlation effects in macroscopic (infinite) and finite (trapped) classical systems and outline peculiarities of the latter. Finally, we also briefly discuss how these effects change in quantum systems where the analysis is substantially more complicated.

Generally, a plasma is considered strongly correlated (or strongly coupled) when the nearest-neighbor interaction energy is on the order of (or exceeds) the thermal energy k_BT. Strong correlations between the constituent particles then give rise to many unique phenomena. Such conditions are important for many processes in, e.g., dense astrophysical objects [6,7], fusion research [4], and the exotic quark-gluon plasma created in ultra-relativistic collisions of nuclei [42,43]. With regards to basic research, the realization of strongly coupled dusty plasmas opens up the possibility to observe liquid and solid state processes at an "atomistic" scale [3]. These experiments carry the promise of making available direct tests of fundamental physical theories such as the topological phase transition in the KTHNY scenario [44–46].

To enable an accurate interpretation of these particle-resolved experiments and to make reliable predictions, naturally, requires a thorough theoretical description and a detailed understanding of the fundamental processes that are involved in the physics of correlation phenomena. Here one has to clearly distinguish between generic correlation effects and specifics of individual systems. While the former are a consequence of the pair interaction between the plasma particles and of the system geometry including

* Contribution to the Topical Issue "Fundamentals of Complex Plasmas", edited by Jürgen Meichsner, Michael Bonitz, Holger Fehske, and Alexander Piel.

[a] e-mail: ott@theo-physik.uni-kiel.de

dimensionality and confinement effects, the latter depend on many details of the plasma generation mechanism. For the example of dusty plasmas, this includes the discharge geometry or frequency and the presence of electric fields that give rise to flows of charged or neutral particles that are, ultimately, associated with nonequilibrium effects such as wakes. These induce substantial departures from pure correlation effects in thermodynamic equilibrium.

Restriction to the "generic" properties obviously leads to a model system. Its main advantage is that it exhibits many key trends that arise from correlation effects that should be important for all strongly coupled plasmas.[1] The most important "quintessential plasma model" to describe correlation effects is the one-component plasma (OCP). In its basic formulation, the OCP is a spatially homogeneous collection of classical, non-relativistic point particles of uniform mass and charge embedded in a neutralizing background of opposite charge. This background can be assumed either unpolarizable, leading to a bare Coulomb interaction between the constituent particles, or weakly polarizable, leading e.g., to the familiar Debye-Hückel or Yukawa screening. The OCP, as a model for real plasmas, is of similar importance as the hard sphere model of real gases or the jellium model for electrons in metals [47,48]. These models play the same conceptual role – to elucidate the fundamental physics which are also at work in more complex systems.

For this reason, in this paper we concentrate on results for the OCP. Its basic parameters and the generalization to quantum systems are introduced in Section 2. Structural properties and phase transitions in the classical and quantum OCP, as well as the specifics of confined systems, are discussed in Section 3. Dynamical and transport properties of infinite and finite system are then reviewed in Section 4.

2 Basic parameters

In the following, the OCP and some important parameters for classical and quantum systems are briefly introduced. For more details, we refer the reader to the available monographs by Ichimaru [49,50] and our recent reviews [3,51]. Furthermore, the main parameters and quantities are summarized in Table 1 where classical and quantum systems, on the one hand, and macroscopic and finite systems, on the other, are compared.

The degree of correlations in a system is typically measured as the ratio between the average potential and kinetic energy per particle,

$$\Gamma = \frac{|\langle V \rangle|}{\langle K \rangle}. \tag{1}$$

For Coulombic systems,[2] $\langle V \rangle$ is conventionally approximated by the two-particle interaction energy at the Wigner-Seitz radius a, which follows from the definition of the number density $n = 3/(4\pi a^3)$, cf. equation (2) and Table 1.

2.1 Classical system in equilibrium

In a classical system in thermal equilibrium, the mean kinetic energy is of the order of $k_B T$ so that

$$\Gamma = \frac{q^2}{a} \times \frac{1}{k_B T} \tag{2}$$

with particle charge q and system temperature T. Note that this *Coulomb coupling parameter* – even though it is commonly used – does not take the actual average potential energy per particle into account – it disregards both the interaction energy associated with long-range interaction and the number of nearest neighbors. Consequently, the main advantage of the parameter Γ is that it reflects the correct scaling of Coulomb interaction effects with the relevant system parameters: temperature, charge, and density. At the same time, its absolute value is not of universal importance. Most importantly, Γ is the only parameter needed to completely describe the system's structural properties and thermodynamic phases. We also note that another interpretation for Γ can be given as $\Gamma = l_L/a$, i.e., the ratio of the Landau length $l_L = q^2/k_B T$ and the Wigner-Seitz radius a. In this view, $l_L = \Gamma a$ is the distance at which the potential energy between two particles equals their thermal energy.

For Debye-Hückel/Yukawa systems ("Yukawa OCP") with interaction potential

$$V_Y(r) = \frac{q^2}{r} e^{-r/\lambda} \tag{3}$$

it is customary to employ the same Coulomb coupling parameter Γ as for pure Coulomb systems. Evidently, in this case Γ serves even more as a convenient normalization than as a physically relevant parameter. Since the potential (3) is not scale-free, an additional parameter is needed which quantifies the screening length λ. This parameter will be written below as $\kappa = a/\lambda$, the ratio of the Wigner-Seitz radius to the screening length. An improved definition of the coupling parameter for a Yukawa OCP, Γ^{eff}, will be introduced in Section 3.1. The screening length itself depends on the screening mechanism present in the system considered and differs between classical and quantum systems where it equals the Debye and Thomas-Fermi length, respectively. In the following, we will use κ as an additional parameter that governs the interaction range of the potential. In the limit $\kappa \to 0$, we will recover the Coulomb potential.

2.2 Equations of motion of a classical strongly coupled plasma

To describe the dynamics of the OCP an additional parameter (besides Γ) is needed which arises from the particle mass m. This mass dependence defines a relevant time scale, which is given by the inverse of the plasma frequency, $\omega_p^{-1} = \sqrt{a^3 m/(3q^2)}$, cf. Table 1. The equations of

[1] At the same time, the neglect of specific features has to be verified and justified, in each case, before the results are applied to real systems.

[2] The *cgs*-system of units is used throughout this work.

Table 1. Overview of parameters and key properties of strongly correlated one-component plasmas in thermodynamic equilibrium (unmagnetized, unscreened, $\kappa = 0$): I. Relevant length and time scales. II. Common dimensionless parameters. III. Thermodynamic functions, including: free energy F, entropy S, heat capacity c, pair distribution g and s-particle distribution. IV. Phase transitions. V. Collective excitations. VI. Transport properties. The relevant sections and equations are indicated. The modifications due to screening of the interaction and in a magnetic field are discussed in the main text. Spin properties are specified for the case of fermions with $s = 1/2$. For topics not covered in this article, the reader is referred to the indicated references and literature cited therein.

Charge q, Mass m, Temperature T	**Classical system**	**Quantum system ("jellium")**
Infinite system	I. Length: a; $l_L = \frac{q^2}{k_B T}$ (Landau length) Time: $t_0 = \omega_p^{-1}$ Energy: q^2/a; $k_B T$	I. Length: a; $\Lambda = h/\sqrt{2\pi m k_B T}$; $a_B = \frac{\hbar^2}{mq^2}$ Time: $t_0 = \omega_p^{-1}$ Energy: q^2/a; $k_B T$; $E_F = \frac{\hbar^2 (3\pi^2 n)^{2/3}}{2m}$
Homogeneous Density $n = 3/(4\pi a^3)$ a: mean interparticle distance	II. Coupling: $\Gamma = q^2/(a k_B T)$	II. Coupling: $r_s = a/a_B$ Degeneracy: $\Theta = k_B T/E_F$; $\chi = n\Lambda^3$ Spin polarization: $\xi = \frac{N_\uparrow - N_\downarrow}{N_\uparrow + N_\downarrow} \in [0, 1]$
Plasma frequency $\omega_p = \sqrt{\frac{4\pi n q^2}{m}}$	III. F, S, c_V, $g(r)$, equation (11) IV. Liquid–solid at $\Gamma = \Gamma_m$	III. F, S, c_V, $g_{\alpha\beta}(r)$, $\alpha, \beta \in \{\uparrow, \downarrow\}$ IV. Liquid–solid at $r_s = r_{sm}$, Spin polarization of fluid: $r_s = r_s^{pol}$, [69]
	V. Plasmons, $\Omega_i(k)$, reference [70] Plasma waves	V. Plasmons, $\Omega_i(k)$, reference [65] Charge density waves, spin density waves
	VI. Diffusion, heat conduction, Section 4	VI. Reference [71]
Trapped system	I. Length: r_0 Time: $t_0 = \omega^{-1}$ Energy: q^2/r_0; $m\omega^2 r_0^2/2$; $k_B T$	I. Length: r_0; $l_0 = \sqrt{\frac{\hbar}{m\omega}}$ Time: $t_0 = \omega^{-1}$ Energy: $\hbar\omega$; q^2/l_0; $k_B T$
	II. Coupling: $\Gamma = q^2/(r_0 k_B T)$	II. Coupling: $\lambda = \frac{q^2}{l_0 \hbar\omega}$ Degeneracy: $\beta = \frac{\hbar\omega}{k_B T}$
Trap frequency ω r_0: mean interparticle distance r_0 : from $\frac{q^2}{r_0} \approx \frac{m\omega^2 r_0^2}{2}$ Inhomogeneous Radial shells (n_i, N_i) Particle number, $N = \sum_i N_i$	III. $g_{n_1,n_2}(\mathbf{r}_1, \mathbf{r}_2)$, $g_{n_1,n_2,n_3}(\mathbf{r}_1, \mathbf{r}_2, \mathbf{r}_3)$ Shell-resolved correlations, Section 3.2 $S_\omega^{(k)}$, $c_\omega^{(k)}$, equations (15) and (16) IV. Radial melting, intra-shell disordering, Section 3.2 V. Normal modes, reference [3] VI. Diffusion, heat conduction, viscosity, Section 5	III. $g_{n_1,n_2}^{\alpha_1,\alpha_2}(\mathbf{r}_1, \mathbf{r}_2), \ldots, g_{n_1,n_2,n_3}^{\alpha_1,\alpha_2,\alpha_3}(\mathbf{r}_1, \mathbf{r}_2, \mathbf{r}_3)$ Shell- and spin-resolved correlations, $\alpha_i \in \{\uparrow, \downarrow\}$ IV. 2D: radial and angular melting, reference [72] 3D: open V. Normal modes, Section 5.2 VI. Diffusion, reference [67]

motion for the particles $i = 1, \ldots, N$ for the Yukawa OCP read

$$m\frac{d^2}{dt^2}\boldsymbol{r}_i = -\nabla_{\boldsymbol{r}_i}\sum_{i\neq j}^{N}\frac{q\exp(-r_{ij}/\lambda)}{r_{ij}} + \frac{q}{c}\frac{d}{dt}\boldsymbol{r}_i \times \boldsymbol{B}, \quad (4)$$

where an external magnetic field $\boldsymbol{B}$ has been added which is directed along the unit vector $\hat{\boldsymbol{e}}_B$. Introducing dimensionless lengths and times, $\boldsymbol{\rho}_i = \boldsymbol{r}_i/a$, $\rho_{ij} = r_{ij}/a = |\boldsymbol{r}_i - \boldsymbol{r}_j|/a$, and $\tau = t\omega_p$, these equations are rewritten in dimensionless form,

$$\frac{d^2}{d\tau^2}\boldsymbol{\rho}_i = -\frac{1}{3}\nabla_{\boldsymbol{\rho}_i}\sum_{i\neq j}^{N}\frac{\exp(-\kappa\rho_{ij})}{\rho_{ij}} + \beta\frac{d}{d\tau}\boldsymbol{\rho}_i \times \hat{\boldsymbol{e}}_B, \quad (5)$$

where the magnitude of the magnetic field is given by $\beta = \omega_c/\omega_p$ [$\omega_c = qB/(mc)$ is the cyclotron frequency]. For $\kappa = 0$ ($\lambda = \infty$), these equations correspond to the equations of motion for the (Coulomb) OCP.[3] For a finite system in a trap, we have to include in equation (4) additionally the confinement force $|\mathbf{F}_i^c| = -m\omega^2 r_i$ acting on each particle radially towards the trap center.

2.3 Quantum charged particle system in equilibrium

When quantum effects of the charged particles become relevant (at low temperature and/or high density), the previous description breaks down. A quantitative characteristics is given by quantum degeneracy parameters. Two commonly used parameters are

$$\chi = n\Lambda^3 = \frac{3}{4\pi}\left(\frac{\Lambda}{a}\right)^3 \approx 0.24\left(\frac{\Lambda}{a}\right)^3, \quad (6)$$

$$\Theta = k_B T/E_F = \frac{4\pi}{(3\pi^2)^{2/3}}\chi^{-2/3} \approx 1.31\,\chi^{-2/3}, \quad (7)$$

[3] We note that for planar systems, the system units are given by $a = 1/\sqrt{\pi n}$ (where n is the areal number density) and $\omega_p^{-1} = \sqrt{a^3 m/(2q^2)}$, whereas the definitions for Γ and κ remain unchanged.

where Λ is the thermal de Broglie wavelength and E_F is the Fermi energy, see Table 1. Quantum effects are small for systems characterized by $\ell = \Lambda/a \lesssim 0.2$, $\chi \lesssim 0.05$, or $\Theta \gtrsim 10$ (these inequalities are approximately equivalent).

When quantum effects are not negligible, the classical OCP has to be replaced by the more general "jellium model" (also known as uniform electron gas, UEG) [47,48]. In contrast to the OCP, its complete structural description (apart from the spin polarization) requires two parameters, Γ and Θ. However, it is common to consider the pair (Θ, r_s) instead, where the Brueckner parameter r_s is the ratio of the Wigner-Seitz radius a and the Bohr radius

$$r_s = \frac{a}{a_B} = \left(\frac{81\pi^2}{128}\right)^{1/3} \Theta\Gamma \approx 1.84\,\Theta\Gamma. \tag{8}$$

Note that, due to the high current interest in matter under extreme conditions ("warm dense matter", where $r_s \sim \theta \sim 1$ [52]), there has been a spark in thermodynamic simulations of jellium, e.g., references [25,28,31,33–36,38–40,53–63], and an accurate, complete thermodynamic description of its properties was achieved only recently [33,36], see reference [64] for a recent review.

To facilitate comparisons between the quantum UEG (Θ, r_s) and the classical OCP (Γ), the following relations are convenient,

$$\Gamma = \left(\frac{128}{81\pi^2}\right)^{1/3} \frac{r_s}{\Theta} \approx 0.54\frac{r_s}{\Theta}, \tag{9}$$

$$\ell = \frac{\Lambda}{a} = \left(\frac{2^{5/2}\pi^{1/4}}{3}\right)^{2/3} \frac{1}{\sqrt{\Theta}} \approx 0.54\frac{1}{\sqrt{\Theta}}. \tag{10}$$

The dynamics of correlated quantum systems are much more complicated than the classical analogue. Here, substantial progress has recently been achieved using quantum kinetic theory [65] and nonequilibrium Green functions [66–68]. Some quantum dynamics results will be presented in Section 5.

3 Structure and phase transitions

In this section, the structural properties of the OCP[4] are investigated. We develop criteria which classify the coupling strength in the plasma and show that a meaningful comparison between differently screened Yukawa systems is possible by defining a modified coupling parameter. We also demonstrate a method for resolving phase transitions in finite systems for which bulk criteria are not applicable.

3.1 Extended systems

For macroscopic (infinitely extended) systems, a suitable microscopic measure of correlation effects is the radial pair distribution function (RPDF) $g(r)$ that is defined as the angle-average of the two-particle distribution function $g(\boldsymbol{r})$,

$$g(\boldsymbol{r}) = \frac{1}{Nn}\left\langle \sum_{i\neq j}^{N} \delta(\boldsymbol{r} - \boldsymbol{r}_{ij}) \right\rangle. \tag{11}$$

The RPDF is a central quantity for the thermodynamics of the OCP since it determines all static properties, e.g., the compressibility, the energy, or the pressure [73]. It is also a means to incorporate particle correlation into analytical theories such as the quasi-localized charge approximation [74].

In an ideal system, $g(r) \equiv 1$, indicating the absence of any spatial order. As the non-ideality increases, the so-called correlation hole (depletion of $g(r)$ at small pair separations) appears for repulsive potentials. A second feature of the RPDF manifests itself at larger particle correlations, viz. a series of peaks and troughs corresponding to a shell-like arrangement of neighbors. Together, these two features allow one to classify systems into uncorrelated (no correlation hole), weakly correlated [finite correlation hole but no peaks in $g(r)$], and strongly correlated [distinct peaks in $g(r)$].

Sensitive measures for the correlation hole and the degree of correlation are the value $r_{1/2}$, at which $g(ar_{1/2}) = 1/2$, and the height, $g_{\max}$, of the first peak of the RPDF [15,76]. Using these characteristics, it is possible to define a mapping between the structural properties of systems with different interaction potentials. This is particularly interesting for the comparison of Coulomb systems and Yukawa systems with different screening lengths. This strategy allows one to define an effective coupling parameter $\Gamma^{\text{eff}}(\kappa)$ for a Yukawa system which coincides with Γ defined in equation (2), for $\kappa = 0$, and gives the structurally most similar Yukawa system for a given finite κ. The result is (details can be found in reference [15]):

$$\Gamma^{\text{eff}}(\Gamma, \kappa) = f(\kappa)\cdot\Gamma, \quad 0 \le \kappa \le 2,\ 1 \le \Gamma^{\text{eff}} \le 150, \tag{12}$$

where the scaling function is given by

$$f(\kappa) = 1 - 0.309\kappa^2 + 0.0800\kappa^3. \tag{13}$$

Although formally outside the definition range of Γ^{eff}, the value $\Gamma^{\text{eff}} = 172$ can be used as an universal melting point for Coulomb and Yukawa OCP, see Figure 1. This underlines the universality of the melting process in (Yukawa) OCPs. The definition (12) utilizes only some of the information contained in the RPDF. A more specific matching between the OCP and experimental systems is possible by also taking into account the positions and heights of the additional extrema of the RPDF. These have been published in tabular form for two- and three-dimensional systems in reference [21].

3.1.1 Quantum and spin effects

We conclude this section by considering the impact of quantum effects. In Figure 2, the RPDF of a classical OCP and a quantum UEG at comparable coupling and

[4] The term OCP is meant here to include both Yukawa and Coulomb interacting systems.

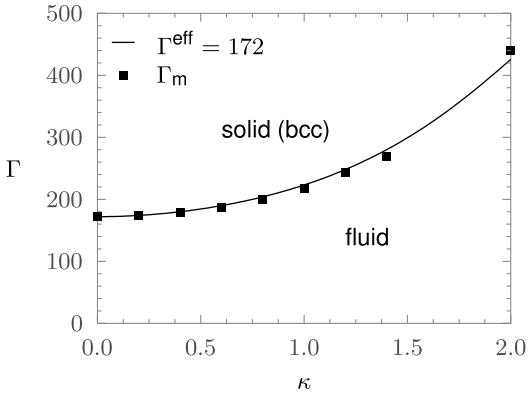

Fig. 1. κ–Γ phase diagram for Yukawa systems. The symbols indicate the melting transition [75]. The solid line marks a constant effective coupling parameter $\Gamma^{\text{eff}} = 172$. Note that for larger κ the phase diagram is more complex due to the existence of an additional fcc-lattice phase (not shown) [75]. Reprinted from reference [15].

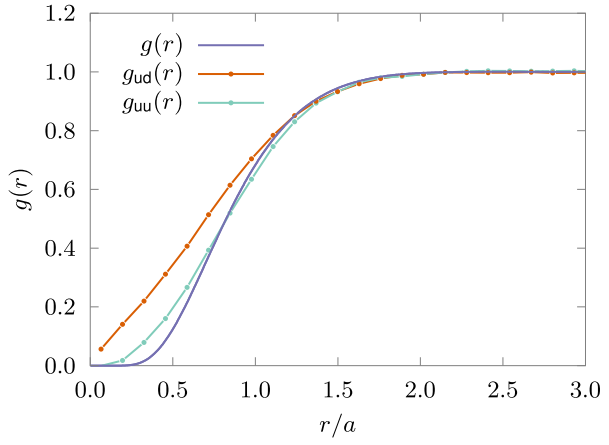

Fig. 2. Pair distributions of a one-component system. $g_{uu} = g_{\uparrow\uparrow}(r)$ and $g_{ud} = g_{\uparrow\downarrow}(r)$: spin-resolved RPDFs of the quantum UEG at $r_s = 4$ and $\Theta = 1$ ($\Gamma = 2.16$ and $\ell = \Lambda/a = 0.54$). $g(r)$: RPDF of the classical OCP at $\Gamma = 2$. Data from references [15,28].

moderate degeneracy are visualized. The UEG data are calculated by *ab initio* permutation blocking path-integral Monte Carlo simulations (PBPIMC approach [25,26]) and are spin-resolved for electrons with parallel ($\uparrow\uparrow$) and anti-parallel ($\uparrow\downarrow$) spins. The larger correlation hole for electrons with parallel spin is a consequence of the Pauli principle (two electrons with same spin projection cannot occupy the same spot, even in the absence of pair interaction). Of course, this effect is absent for different spins. Since the UEG considered here was unpolarized (zero total spin projection, $\xi = 0$, cf. Tab. 1), the mean pair distribution function is, in good approximation, $g_{\text{UEG}}(r) = \frac{1}{2}[g_{\uparrow\uparrow}(r) + g_{\uparrow\downarrow}(r)]$ (not shown). As can be seen in Figure 2, quantum effects reduce correlations compared to the classical case [compare $g_{\uparrow\uparrow}(r)$ and $g(r)$], since the quantum delocalization decreases the correlation hole and "smears out" the pair correlations, even in the presence of the Pauli repulsion.

3.2 Finite systems

Finite clusters of charged particles have been extensively analyzed in recent years in dusty plasmas or trapped ions after their successful creation in suitable confinement potentials. The competition of a confinement potential and the Coulomb interaction between the particles typically leads to the formation of concentric shells (or rings in 2D). The properties of these finite clusters and especially phase transitions comprise many complex features [77] related to, e.g., the occurrence of highly symmetric "magic" clusters (for certain particle numbers N) which are particularly stable against melting [78,79]. Obviously, the transition from a crystal-like state, with complete localization of particles, to a liquid-like state involves the loss of order within individual shells (intrashell disordering, ID), relative angular disordering of two shells, and radial melting (RM) where a particle undergoes transitions between two shells [80,81]. All these transitions, in general, occur at different temperatures (different coupling parameters), i.e., in contrast to macroscopic systems, instead of a single melting transition, here one should expect a series of phase transitions. While this has been analyzed in detail for finite 2D clusters [79,80], 3D clusters are much more complex, and only partial results are available, e.g., references [24,78,82].

A complete understanding of these complex properties requires a criterion for the occurrence of phase transitions which is able to resolve different stages of the melting process. Furthermore, to compare with experiments that detect the coordinates of individual particles, it is desirable to formulate such a criterion exclusively in coordinate space. Finally, a system in a trap is spatially inhomogeneous (cf. top part of Fig. 3), thus its properties, including correlation effects, vary in space. This means, the key quantity used in macroscopic systems, the pair distribution function $g(r)$, has to be generalized. An obvious choice is the two-particle distribution function $g_{n_1,n_2}(\mathbf{r}_1, \mathbf{r}_2)$ that describes the probability to find a particle pair at position $\mathbf{r}_1$ and shell n_1 and $\mathbf{r}_2$ and shell n_2, respectively. It turns out that this is not always sufficient, and also the three-particle function $g_{n_1,n_2,n_3}(\mathbf{r}_1, \mathbf{r}_2, \mathbf{r}_3)$ may be required.

A systematic approach to these quantities was developed in reference [24]. It starts from the full N-particle equilibrium distribution function, ρ, and introduces reduced k-particle distributions ($k = 1, \ldots, N-1$) by integrating out the remaining $N - k$ positions:

$$\rho_k(\boldsymbol{r}_1, \ldots, \boldsymbol{r}_k) = \frac{1}{(N-k)!} \int \mathrm{d}^3 r_{k+1} \ldots \mathrm{d}^3 r_N \rho(\boldsymbol{r}_1, \ldots, \boldsymbol{r}_N), \tag{14}$$

where ρ is normalized to $N!$. The problem simplifies substantially by exploiting the spherical symmetry of the system and by relating the k-particle distribution of the correlated system to the one of the non-interacting system, ρ_k^{id}, which gives rise to the reduced correlation function $g_k = \rho_k / \rho_k^{\text{id}}$. As an illustrative example, we show in Figure 3 a modified two-particle correlation function – the center-two-particle correlation function (C2P). Shown is

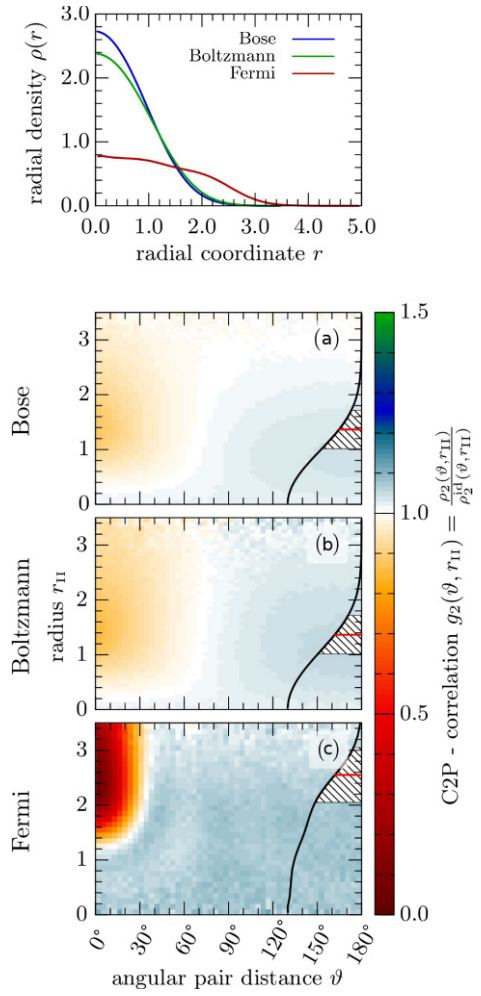

Fig. 3. Distribution, correlations and quantum and spin effects of $N = 13$ particles in a harmonic trap with $\beta = 3$ and $\lambda = 0.1$, cf. Table 1. *Top*: Radial density profile for the case of spinless particles ("Boltzmann", green), Bose statistics (blue), and Fermi statistics (red). *Bottom*: Corresponding center-two particle correlation functions averaged over the outer region of the density profile (see shaded area in the insets) for bosons (a), distinguishable particles (b), and fermions (c). Reproduced from Dornheim et al. [32]. Copyright Wiley-VCH Verlag GmbH & Co. KGaA. Reproduced with permission.

the probability of finding one particle at a certain distance from the trap center (vertical axis) and a second one in the outer "shell" (shaded area under the density profile), aligned under a given angle (horizontal axis) relative to each other. Focusing on part (b) one clearly sees a decreased correlation of particles within the same shell and an angular distance smaller than 20° (the so-called (exchange-) correlation hole). This is typical for the case of moderate correlation whereas for lower temperatures (strong correlations) more and more localization features emerge indicating a transition to a crystal-like state. A similar analysis can be performed for the three-particle correlation function (TCP) that is derived from ρ_3. For details and the involved coordinate transforms, the reader is referred to reference [24].

Of course, the information contained in the C2P and TCF is very detailed and comprehensive as it resolves all relevant distances between particles. In order to derive a criterion that can be used to obtain the phase boundaries, we define reduced Shannon entropies, $S^{(k)}$, according to [24],

$$S^{(k)} \sim -k_B \frac{(N-k)!}{N} \int \mathrm{d}^3 r_1 \dots \mathrm{d}^3 r_k \; \rho_k(\boldsymbol{r}_1, \dots, \boldsymbol{r}_k) \times \ln \rho_k(\boldsymbol{r}_1, \dots, \boldsymbol{r}_k) \tag{15}$$

from which we derive an effective "heat capacity"

$$c_\omega^{(k)} \equiv T \left.\frac{\partial S^{(k)}}{\partial T}\right|_\omega = - \left.\frac{\partial S^{(k)}}{\partial \ln \Gamma}\right|_\omega, \quad k = 1, 2, 3, \dots \tag{16}$$

of the kth correlation function. Note that the harmonic trap gives rise to a modified "canonical ensemble" where the parameters N, V, T are replaced by N, ω, T, and derivatives in equation (16) are computed at fixed trap frequency (and N). Results for a classical Coulomb cluster of $N = 80$ particles in 3D are shown in Figure 4 and demonstrate the remarkable power of this approach to identify the different disordering processes: as for phase transitions in macroscopic systems, peaks of the generalized heat capacities are a clear signal of enhanced fluctuations that are characteristic of an disordering transition. Which transition takes place is understood by analyzing simultaneously the peaks of the heat capacities associated with the single particle distribution (i.e. the density), the two-particle and three-particle correlation functions and entropies or heat capacities.

3.2.1 Quantum and spin effects

The developed approach to phase transitions in finite systems can be straightforwardly extended to quantum systems. This is illustrated in the following for quantum particles in a parabolic trap with trap frequency ω. In particular, to investigate the effect of quantum statistics on spatial correlations, we consider (spin-polarized) bosons and fermions and, as a reference, spin-free "distinguishable" particles (so-called Boltzmannons). In the fermionic case, this model system is often used as a description for electrons in a quantum dot, e.g., references [72,83–87]. Figure 3 shows results for $N = 13$ quantum particles at weak coupling and relatively low temperature (for definitions, cf. Tab. 1), $\beta = 3$ and coupling constant $\lambda = 0.1$ [32]. Under these conditions, the particle wave functions overlap, and the effects of quantum statistics distinctively manifest themselves in the radial density profiles (top panel). Compared to the distinguishable (spinless) particles (green), bosons (blue) are more concentrated around the center of the trap (as this reduces their energy) whereas fermions (red) are pushed outward, due to the Pauli principle.

In the bottom panel, we show the corresponding C2P functions that are averaged over the outer region of the density profile. Evidently, bosons (a) and distinguishable particles (b) exhibit a fairly similar behavior and the

exchange-correlation hole around $\vartheta = 0$ is only weakly expressed. In stark contrast, for fermions (c), there is a pronounced region where the probability of finding another electron is severely decreased. Therefore, the analysis has revealed that, at the present conditions of weak coupling, correlation effects of quantum confined electrons are dominated by Fermi statistics (and, hence, the Pauli repulsion) and only weakly influenced by the weak non-ideality. This emphasizes the important role correlation functions play for the understanding of the nontrivial interplay of quantum exchange and Coulomb correlation effects in non-ideal quantum systems. Details can be found in reference [32].

4 Dynamics and transport in correlated plasmas

The dynamics of strongly coupled classical magnetized plasmas represent a particular challenge for theory since the large role played by interparticle interactions necessitates a particle-based description, and the presence of a magnetic field introduces further complexity. In this section, we review the recent progress made by the SFB TR-24 in elucidating important transport processes in these systems, viz., heat transport, momentum transport (viscosity), and mass transport (diffusion).

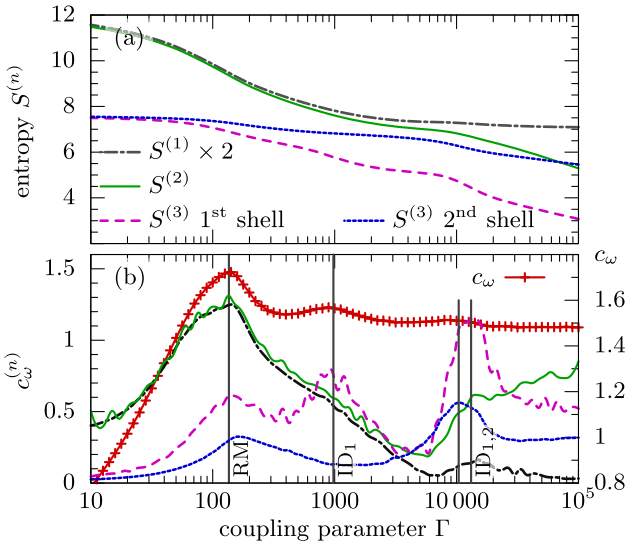

Fig. 4. Top: Reduced entropies of the one-particle distribution [$S^{(1)}$], two-particle distribution C2P [$S^{(2)}$] and TCF [$S^{(3)}$, shell-resolved] as a function of Γ for a Coulomb cluster of $N = 80$ particles. Bottom: Heat capacities $c_\omega^{(k)}$ corresponding to the reduced entropies of (a) compared to the conventional thermodynamic heat capacity c_ω (crosses). The peaks of $c_\omega^{(k)}$ (cf. vertical lines) signal disordering transitions [RM: radial melting, ID1/2: intrashell disordering on the inner/outer shell] Reprinted from reference [24].

4.1 Correlation effects on the diffusion properties in a macroscopic system

Diffusion is the most simple transport process. Since it is intimately connected to the motion of individual particles, it lends itself to a detailed analysis. Concomitantly, a particle-based exploration of the system dynamics can help to identify the "building blocks" of more complex processes involving many particles simultaneously. Molecular dynamics allows for a direct approach to the diffusion coefficient by computing the mean-squared displacement (MSD) that is averaged along the trajectories of all particles, $u_r(t) = |\langle \boldsymbol{r}_i(t) - \boldsymbol{r}_i(0)\rangle_N|^2$. A typical result is shown in Figure 5, see curve $\beta = 0$ in the top part. At early times, the particles move ballistically, $u_r(t) \sim t^2$, while diffusive motion, $u_r(t) \sim t^1$, occurs at larger time delays, where the slope is proportional to the diffusion coefficient. An interesting peculiarity is observed in 2D Yukawa systems. There, superdiffusion was observed experimentally in dusty plasmas [88] and in simulations [89] which is related to a growth of $u_r(t)$ faster than t^1. However, we could show with accurate MD simulations that this is only a transient phenomenon in these dissipative systems [90–92]. The next interesting question is the effect of Coulomb interaction on the diffusion coefficient. Since the increase of the coupling strength is accompanied by enhanced particle localization, the consequence should be a reduction of the mobility. This is indeed observed in the lower part of Figure 5, cf. the data points for different values of Γ at $\beta = 0$ [93].

4.2 Diffusion in magnetized strongly correlated systems

Let us now turn to the influence of a magnetic field on the diffusion coefficient. This has been studied in great detail for weakly coupled (high-temperature) plasmas where it was found that the cross field diffusion coefficient decays as $1/B^2$, whereas diffusion parallel to the field is independent of the field strength [94]. At very strong fields, anomalous transport sets is in giving rise to a linear reduction of the mobility perpendicular to the field, $D_\perp \sim 1/B$, that was first observed by Bohm.

Now the interesting question arises how the magnetic field acts in a correlated system – which was analyzed for a 3D classical OCP in reference [93] and for 2D systems in reference [14]. In 3D it was found that $D_\perp$ rapidly decays with both B and Γ and, at sufficiently large B always approaches the Bohm regime, $D_\perp \sim 1/B$. A striking result was that also $D_\parallel$ turned out to be field dependent. This is easily understood as correlation effects give rise to large-angle scattering of particles, and particles initially moving parallel to the field may obtain a large velocity component perpendicular to the field. As a result, simulations revealed that, for large Γ also $D_\parallel \sim 1/B$ [93], in striking contrast to high-temperature plasmas.

In two-dimensional systems oriented perpendicular to the B-field, only cross-field diffusion is possible, and the behavior is illustrated in Figure 5. The upper curve shows the MSD for different values of the magnetic field strength [14]. As in the field-free case, at early times,

the particles move ballistically, $u_r(t) \sim t^2$, while diffusive motion occurs at larger time delays. With increasing magnetic field, an oscillatory behavior is imprinted on the MSD by the gyrating motion of the particles. An early sub-diffusive behavior occurs which is replaced with ballistic migration only at later times. The onset of diffusive motion is shifted to larger time delays as well.

After a sufficiently long time, an almost diffusive motion is established, at all magnetic field strengths considered, and a measure of the diffusion can be estimated from $D^* = \lim_{t\to\infty} u_r(t)/(4\,t)$.[5] Results are given in the lower part of Figure 5 for different values of Γ. It is found that the effect of the magnetic field is to suppress the self-diffusion in 2D OCPs. The suppression is different at different field strength regimes: small to negligible reduction, for $\beta < 0.5$, and a Bohm-type $1/\beta$ suppression, at $\beta \gtrsim 1$. In good approximation, the relative suppression of the self diffusion, $R(\beta) = D^*(\beta)/D^*(0)$ is independent of Γ and given by

$$R(\beta) = \frac{1+\beta/3}{1+\frac{7}{4}\beta+\beta^2} \tag{17}$$

from which the α/β decay at large β is evident. Here, $\alpha = 48/71 \approx 2/3$ which is comparable with the decay prefactor in three dimensional system [93,96].

An extension of this analysis two a two-component system of particles with different charge to mass ratio was presented in reference [14] and indicated interesting additional effects such as non-monotonic dependencies of the transport properties on the magnetic field strength which are expected to be highly relevant for future studies of multicomponent plasmas.

4.3 Relation of diffusion to caging effects

Diffusive motion in strongly coupled plasmas is also intimately connected to the mean time that a particle spends in a local potential minimum created by the other particles (so-called "caging time"). A variant of this caging time, the "directional caging time", is shown in Figure 6, for different coupling strengths, as a function of β [29]. The dramatic increase of caging times due to the magnetic field is evident, and this time can be directly related to the diffusion coefficient. It is interesting to note that this caging time can be calculated semi-analytically within the quasi-localized charge approximation for magnetized systems [12,97,98]. For more details, see the contribution by Kählert et al. in this issue [70].

The complexity of the correlation-magnetic field interaction is also manifest in the generation of supercooled 2D Yukawa liquids [13]. If a sufficiently correlated Yukawa OCP is rapidly cooled ("quenched"), structural rearrangement generally leads to a new crystalline equilibrium state, see left path in Figure 7. If a magnetic field is applied to the system, however, the crystallization is blocked since the energy equilibration channels are reduced and the system cannot relax toward equilibrium, see right paths in Figure 7. Such systems have peculiar properties, including a high mobility at low temperature [13]. The transition from equilibrated to non-equilibrated liquids depends critically on the magnetic field: In Figure 8, this is demonstrated for a model system in which a minute increase of the magnetic field leads to a transition in the nature of the particle dynamics. For the quenched magnetized Yukawa OCP, this means that the equilibration timescale is reduced by more than three orders of magnitude when the applied magnetic field is doubled from $\beta = 0.55$ to 1.1 [13].

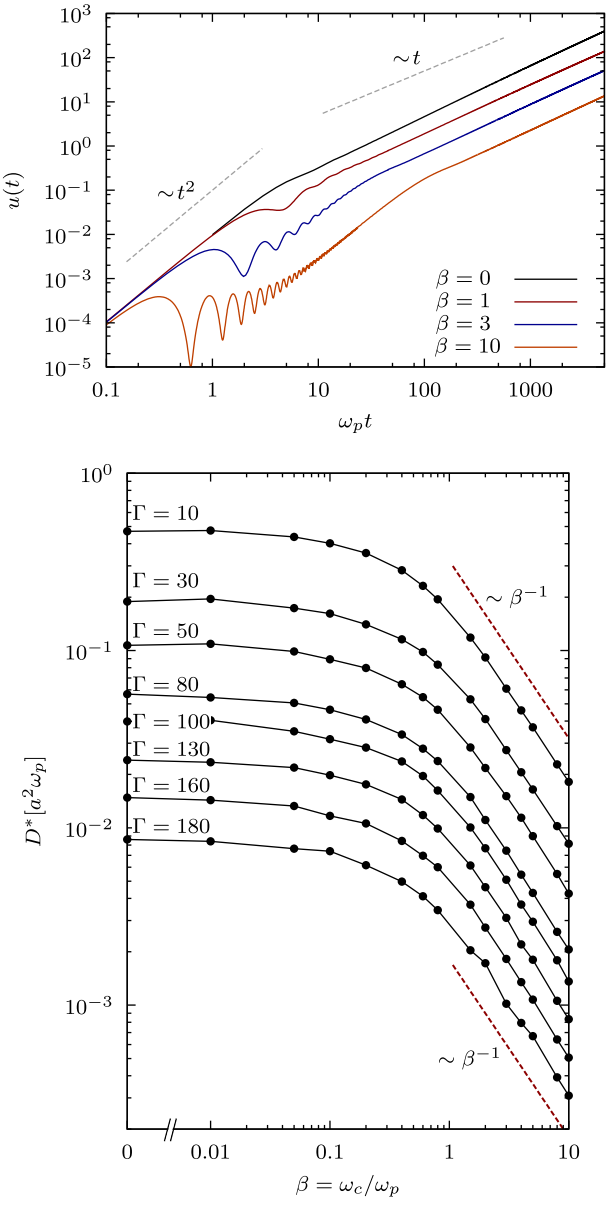

Fig. 5. Top: Mean-squared displacement (MSD) of a 2D Yukawa OCP ($\kappa = 1.0$) at different magnetic fields. The magnetic field imprints an oscillatory MSD and an intermediate sub-diffusive regime. Bottom: A measure of the diffusion coefficient, D^*, and its dependence on Γ and β. The decay with β follows a Bohm-type law $\sim \beta^{-1}$. Reprinted from reference [14].

[5] See reference [95] for an in-depth discussion of anomalous diffusion in 2D magnetized plasmas.

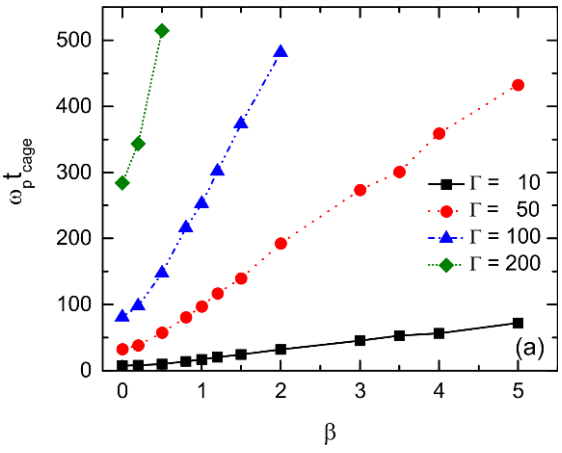

Fig. 6. Directional caging time of particles as a function of the magnetic field strength and Γ, as indicated. See reference [29] for a discussion. Reprinted from reference [29].

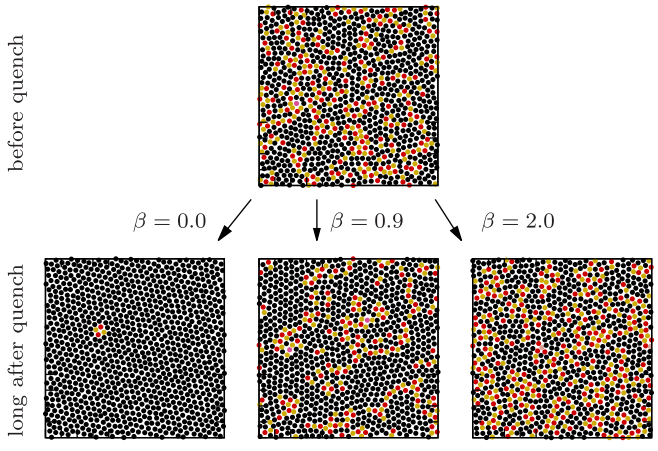

Fig. 7. Results from quenching a 2D Yukawa OCP ($\kappa = 1$, $\Gamma = 140$). The system is initially in the liquid state (top, $\omega_p t = 0$) as is apparent from the system order (the colors code the number of nearest neighbors: 5 [light grey/yellow], 6 [black], 7 [dark grey/red], and other [purple]). The quench is realized by removing all kinetic energy from the system. Depending on the applied magnetic field strength, the system crystallizes ($\beta = 0$) or stays in increasingly long-lived supercooled metastable states (bottom row, $\omega_p t = 24000$). Reprinted from reference [13].

4.4 Heat conductivity in a strongly coupled magnetized OCP

For many plasma applications including thermal transport in stars or fusion, the heat conductivity of a plasma is of crucial importance since it is relevant for the evolution of the energy density and temperature [99]. For the OCP, the heat conduction has been thoroughly investigated in the last decades, see, e.g., references [100,101]. These results have been improved and extended to magnetized systems in references [22,30].

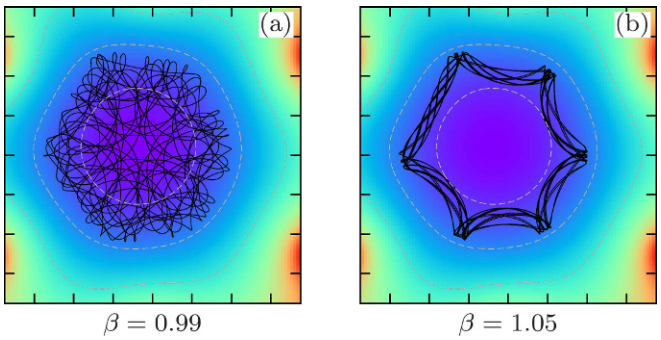

Fig. 8. Trajectory of a particle in an asymmetric cage of six fixed neighbors. At $\beta = 0.99$, the particle can reach all of the energetically accessible regions. At an only slightly larger strength of the magnetic field, $\beta = 1.05$, the congruence between the Larmor radius and the structural arrangement causes a sudden change in the dynamics and the particle is unable to reach the potential minimum. Reprinted from reference [13].

In a magnetized system, Fourier's law must be taken in its tensorial form, i.e.,

$$j_\alpha = -\lambda_{\alpha\beta}(\nabla T)_\beta,$$

where $\boldsymbol{j}$ is the energy flow and the thermal conductivity tensor $\lambda_{\alpha\beta}$ has three independent components (assuming $\boldsymbol{B} \parallel \hat{\boldsymbol{e}}_{\boldsymbol{z}}$),

$$\underline{\underline{\lambda}} = \begin{pmatrix} \lambda_\perp & \lambda_\times & 0 \\ -\lambda_\times & \lambda_\perp & 0 \\ 0 & 0 & \lambda_\parallel \end{pmatrix}. \tag{18}$$

Field-parallel and cross-field heat transport are described by the components $\lambda_\parallel$ and $\lambda_\perp$, respectively. Both reduce to the scalar heat conductivity in the limit of a vanishing magnetic field. In addition, there exists a cross-term, $\lambda_\times$, describing heat currents perpendicular to the temperature gradient (so-called Righi-Leduc effect [103], which is analogous to the Hall effect). In the limit of zero magnetic field isotropy is restored, and the tensor has only a single component λ_0 with $\lambda_\parallel \to \lambda_0$, $\lambda_\perp \to \lambda_0$ and $\lambda_\times \to 0$.

Results for these quantities are given in the top and middle part of Figure 9, as a function of Γ at different magnetic field strengths. The first striking feature is the non-monotonic Γ-dependence of the heat conduction in the absence of a magnetic field, i.e. λ_0. This arises from the interplay of two main mechanisms to the heat conduction: single-particle motion (related to diffusion) and collective modes (phonon-like transport). While the former effect decreases with Γ (as does the diffusion coefficient), the latter rapidly increases and starts to dominate the heat transport resulting in the formation of a minimum of λ_0 around $\Gamma = 40$.

The second striking feature is observed in a magnetized system: the magnetic field may enhance heat transport along the field, i.e. $\lambda_\parallel$. This effect has a two-fold origin. On the one hand, collisional transport of heat is enhanced because the lateral escape of colliding particles

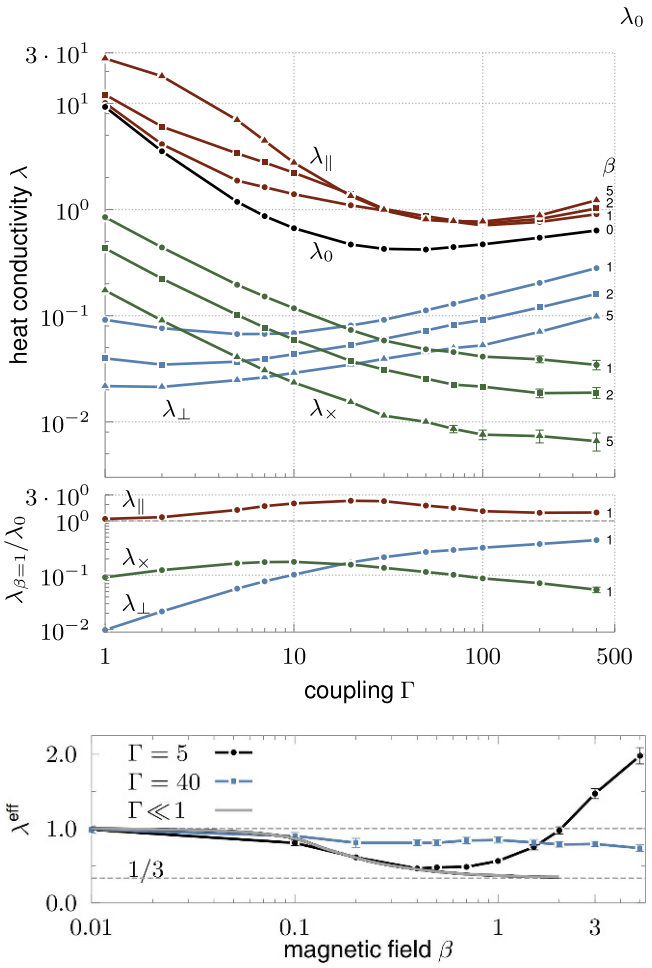

Fig. 9. Top: Elements of the heat conductivity tensor of a Yukawa OCP ($\kappa = 2$) at different magnetic field strengths as a function of Γ. *Middle*: Tensor elements at $\beta = 1$ relative to the field-free value λ_0. Bottom: The effective heat conductivity $\lambda^{\text{eff}} = \text{Tr}\underline{\lambda}$ as a function of β relative to the field-free value. The weakly coupled case $\Gamma \ll 1$ is shown in grey [102]. Reprinted from reference [30].

is restricted by the magnetic field. On the other hand, the transfer of heat associated directly with a moving particle (potential and kinetic energy) is also enhanced since lateral energy loss is reduced and the particle retains its energy for longer flights. The relative importance of the different heat transfer channels and the opposing trends of $\lambda_\perp$ and $\lambda_\parallel$ with β lead to a non-monotonic field dependence of the effective heat conduction, see lower part of Figure 9. A suitable quantity that combines all heat conductivity components is the trace of the tensor, λ^{eff}, which is shown in the bottom part of Figure 9. It shows a distinct non-monotonic behavior with β with a strong increase for $\beta \gtrsim 0.5$ at intermediate values of Γ. For more details, see reference [22].

Besides heat conduction, a magnetic field also suppresses temperature isotropization in plasmas. In conjunction with the importance of collisional heat transport in strongly coupled plasmas, this leads to the emergence of spontaneous temperature anisotropies in an isotropically

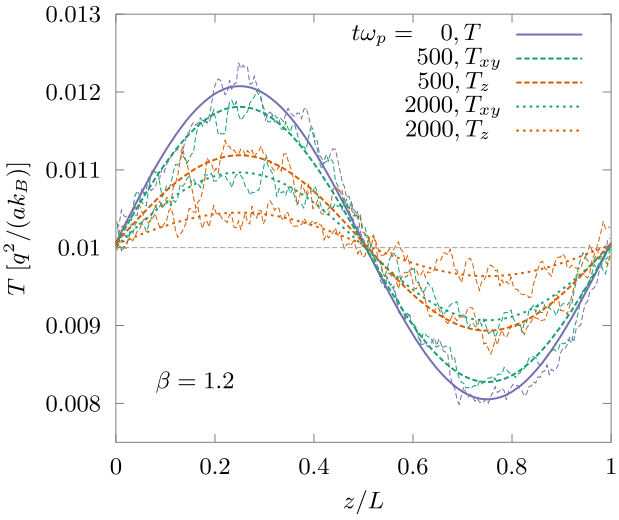

Fig. 10. Field-parallel and cross-field temperature profiles of a Yukawa OCP ($\kappa = 2$, $\Gamma = 100$) after a sinusoidal temperature profile has been imprinted on the system along the field lines, $\boldsymbol{B} \parallel \hat{\boldsymbol{e}}_z$. Shown are the initial temperature profile (solid line) and the profiles at two later times. A temperature anisotropy develops from the isotropic perturbation due to the system dynamics. Reprinted from reference [37].

disturbed plasma [37]. This is illustrated in Figure 10: at $t\omega_p = 0$, an isotropic sinusoidal temperature profile is imposed on the plasma. In the subsequent temporal evolution, the temperature components T_{xy} and T_z relax towards homogeneity with different time dependencies, leading to the described temperature anisotropy. In reference [37], this effect is investigated in detail and an analytical model is developed which describes this behavior.

5 Transport properties of strongly coupled finite plasmas

The calculation of transport properties of finite systems or clusters of particles requires an approach different from that for extended systems since methods based on the fluctuation-dissipation theorem are not straightforwardly applicable. Instead, non-equilibrium methods, in which a gradient is imposed on the systems which leads to a observable flux, closely mimic experimental setups and provide suggestions for future experiments.

5.1 Nonequilibrium approach to heat conduction and viscosity in finite classical systems

For example, the heat transport in a finite 2D dust cluster can be measured by (laser-)heating the central region (shaded region in Fig. 11) and relying on the friction between the dust particles and the surrounding plasma as a heat sink. This non-equilibrium setup leads to a steady-state temperature profile from which the heat conduction properties can be inferred [11,23]: in Figure 11, the radial temperature profiles resulting from different heating laser

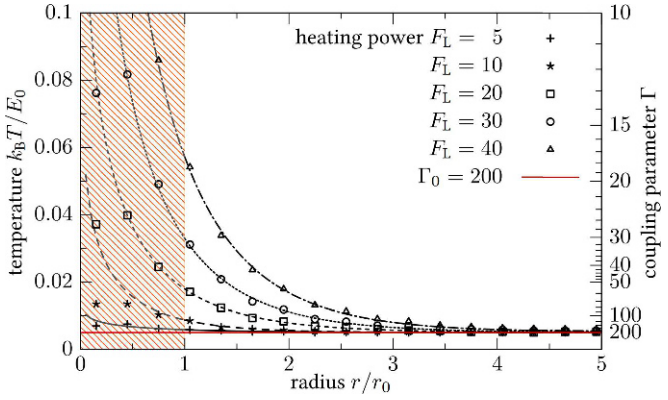

Fig. 11. Temperature profiles of an inhomogeneously heated dust cluster ($\kappa = 1$) for different values of power of the heating laser F_L. Symbols indicate measured temperature profiles and lines the best fit to theory. Reprinted from reference [23].

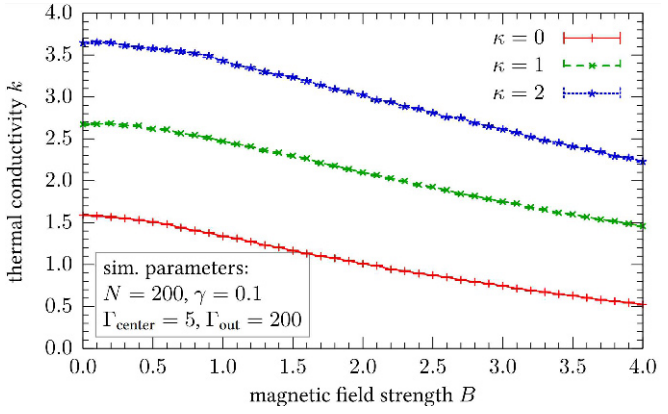

Fig. 12. Thermal conductivity k as a function of the magnetic field strength B for different screening parameters κ obtained from direct non-equilibrium simulation of a heated two-dimensional dust cluster. Reprinted from reference [23].

powers are shown as symbols and the lines correspond to the best fit to the theoretical profiles from which the heat conduction is calculated.

In addition, in this configuration, a perpendicular "effective magnetic field" can be applied by setting the cluster into rotation [8–10]. By measuring the temperature profile and resultant heat conductivity as before, it is found that the magnetic field has the effect of impeding the cross-field heat transfer [23], see Figure 12.

The same principle can be applied to assess the shear viscosity. Here, the laser force is used to imprint a tangential force on the outer ring of particles, see left part of Figure 13, and the velocity profile is measured in radial direction. The viscosity inferred from these simulations [20] is in notably good agreement with macroscopic simulations of extended systems [104] (right part of Fig. 13), which underlines the value of small-cluster experiments.

5.2 Excitations in correlated quantum systems

Finally, we touch upon quantum effects in small spatially confined charged particle systems, e.g., quantum dots [79,81,85], ultracold quantum gases, or quantum particles in traps and optical lattices [105–108]. The simplest dynamic excitations of such systems confined in a parabolic trap are the sloshing (dipole or Kohn) mode [109] and the breathing mode. While the former has the trap frequency, $\omega_{sl} = \Omega$, as in a classical system, the latter – the uniform radial contraction and expansion of all particles – has been found to differ from classical particles. For classical systems (with fixed interaction potential), the frequency of this mode is a constant, independent of the particle number. In the quantum case, however, it depends on the relative strength of the inter-particle interaction λ (see above) and the number of particles N [17,18]. While in the strong coupling limit, $\lambda \to \infty$, the classical result $\omega_{br} = \sqrt{3}\Omega$ is recovered, in the limit of strong quantum degeneracy (strong particle overlap), the ideal quantum gas behavior is obtained where $\omega_{br} = 2\Omega$. These dependencies are shown in Figure 14 for selected values of λ and N.

The measurement of the breathing frequency allows one to determine key observables such as kinetic and interaction energy of a system [16] and is thus particularly well suited as a diagnostic in confined quantum systems, in particular, for electrons in quantum dots, for details see reference [18]. We note that, in addition, the breathing frequency is sensitive to the pair interaction potential – even in classical systems – and the breathing motion may deviate from a self-similar contraction and expansion, e.g., in the case of a Yukawa potential [110]. In the recent years, many computational studies on the breathing mode were performed for ultracold bosonic atoms in traps and optical lattices, e.g. [111–113], because here the corresponding experimental methods are particularly advanced. It can be expected that the collective excitation spectrum will continue to play a crucial role in the understanding and diagnostics of strongly correlated quantum systems in the near future.

6 Summary and outlook

In this paper, we have reviewed recent progress in the theory and simulation of strongly correlated plasmas. The paradigmatic one-component plasma has been used, on the one hand, to gain insight into the fundamental processes occurring in these systems and, on the other hand, to model dusty plasma experiments and develop new experimental protocols and analysis approaches. The structural composition in finite and extended system has been a major research focus over the last decade. Building on this, we have developed criteria for phase transitions in finite clusters that are based on two- and three-article distribution functions, reduced entropies and heat capacities, which elucidate the different stages of disordering in these systems. These techniques have already been used in dusty plasma experiments, and we also demonstrated that they can be successfully applied in the quantum regime as well.

Our second topic was the interplay between a strong magnetic field and particle correlations which was shown to cause non-trivial dynamics. The complexities of this

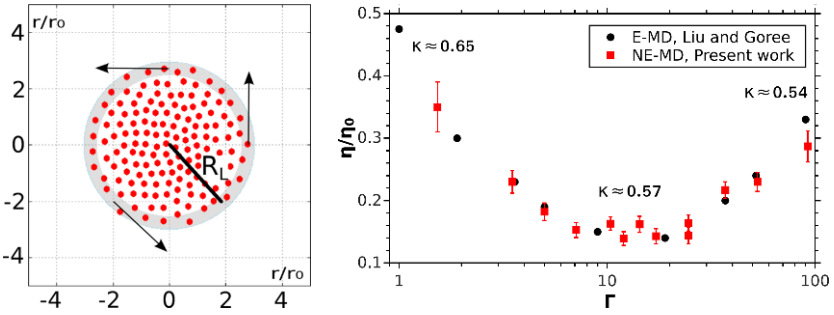

Fig. 13. *Left*: Sketch of the applied non-equilibrium scheme. A tangential force acts on particles inside the shaded ring. *Right*: Viscosity η (in units of $\eta_0 = mn_0\omega_p a^2$ where n_0 is the equilibrium density) inferred from the simulations as a function of Γ, red (light) symbols. The screening varies slightly due to the driving forces as indicated. The dark symbols represent data from Liu and Goree [104] obtained for a periodic dust system. Reprinted from reference [20].

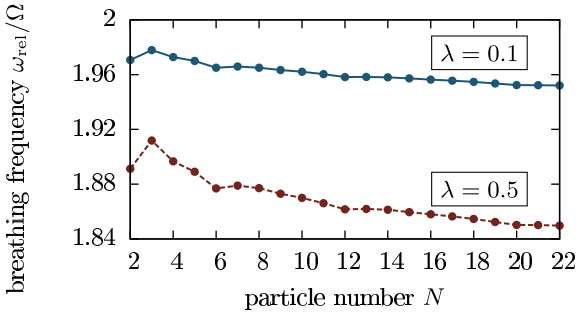

Fig. 14. Breathing frequency of a charged 2D system in a harmonic trap with frequency Ω for two values of the Coulomb coupling parameter λ, cf. Table 1. The result is in striking contrast to classical systems (corresponding to $\lambda \to \infty$) where the breathing frequency equals $\sqrt{3}\Omega$, independently of N. The frequencies of configurations with closed shells ($N = 2, 6, 12, 20$) exhibit local minima. The results were obtained with a sum rule formalism and Hartree-Fock calculations [18].

system have been analyzed through the calculation of tensorial transport coefficients such as the diffusion coefficient, heat conductivity and viscosity, as well as particle-based investigations of the system dynamics following an external excitation. Non-equilibrium methods for small magnetized clusters have been developed which allow for an accurate probing of transport processes, such as diffusion, heat transfer, and viscosity. Previous work in this direction has been complemented by the theoretical and experimental development of rotating dusty plasma experiments (see contribution by Kählert et al. in this issue [70]) which, together with conventional magnetization, allow for unprecedented access to magnetized, strongly correlated systems.

Together, these investigations have furthered the understanding and experimental accessibility of strongly correlated plasmas, in general, and dusty plasmas, in particular, and promise many interesting new results in the near future.

This work has been supported by the DFG through the SFB TR24, projects A5, A7, and A9 and by a grant for CPU time at the HLRN. We thank H. Kählert (Kiel), S. Groth (Kiel), H. Löwen (Düsseldorf), Z. Donkó (Budapest), and P. Hartmann (Budapest) for their contributions to many of the results cited and for interesting and stimulating discussions over the recent years.

Author contribution statement

T.O. (H.T.) designed and executed the studies of the unconfined (confined) classical systems. T.D. contributed the PBPIMC quantum results and J.W.A. those of Section 5.2. M.B. was involved in the conception and discussion of all studies. T.O. and M.B. wrote the manuscript and all authors contributed to the text and graphics of their respective studies.

References

1. T.C. Killian, Science **316**, 705 (2007)
2. I. Bloch, J. Dalibard, W. Zwerger, Rev. Mod. Phys. **80**, 885 (2008)
3. M. Bonitz, C. Henning, D. Block, Rep. Prog. Phys. **73**, 066501 (2010)
4. S.X. Hu, B. Militzer, V.N. Goncharov, S. Skupsky, Phys. Rev. Lett. **104**, 235003 (2010)
5. J.J. Fortney, N. Nettelmann, Space Sci. Rev. **152**, 423 (2010)
6. A.Y. Potekhin, Phys. Usp. **53**, 1235 (2010)
7. A.Y. Potekhin, J.A. Pons, D. Page, Space Sci. Rev. **191**, 239 (2015)
8. H. Kählert, J. Carstensen, M. Bonitz, H. Löwen, F. Greiner, A. Piel, Phys. Rev. Lett. **109**, 155003 (2012)
9. M. Bonitz, H. Kählert, T. Ott, H. Löwen, Plasma Sources Sci. Technol. **22**, 015007 (2013)
10. P. Hartmann, Z. Donkó, T. Ott, H. Kählert, M. Bonitz, Phys. Rev. Lett. **111**, 155002 (2013)
11. G. Kudelis, H. Thomsen, M. Bonitz, Phys. Plasmas **20**, 073701 (2013)
12. T. Ott, D.A. Baiko, H. Kählert, M. Bonitz, Phys. Rev. E **87**, 043102 (2013)
13. T. Ott, H. Löwen, M. Bonitz, Phys. Rev. Lett. **111**, 065001 (2013)
14. T. Ott, H. Löwen, M. Bonitz, Phys. Rev. E **89**, 013105 (2014)
15. T. Ott, M. Bonitz, L.G. Stanton, M.S. Murillo, Phys. Plasmas **21**, 113704 (2014)

16. C.R. McDonald, G. Orlando, J.W. Abraham, D. Hochstuhl, M. Bonitz, T. Brabec, Phys. Rev. Lett. **111**, 256801 (2013)
17. J.W. Abraham, M. Bonitz, C. McDonald, G. Orlando, T. Brabec, New J. Phys. **16**, 013001 (2014)
18. J.W. Abraham, M. Bonitz, Contrib. Plasma Phys. **54**, 27 (2014)
19. H. Thomsen, P. Ludwig, M. Bonitz, J. Schablinski, D. Block, A. Schella, A. Melzer, J. Phys. D: Appl. Phys. **47**, 383001 (2014)
20. S. Landmann, H. Kählert, H. Thomsen, M. Bonitz, Phys. Plasmas **22**, 093703 (2015)
21. T. Ott, M. Bonitz, Contrib. Plasma Phys. **55**, 243 (2015)
22. T. Ott, M. Bonitz, Z. Donkó, Phys. Rev. E **92**, 063105 (2015)
23. H. Thomsen, Melting processes and laser manipulation of strongly coupled Yukawa systems, Ph.D. thesis, Christian-Albrechts-Universität Kiel, 2015
24. H. Thomsen, M. Bonitz, Phys. Rev. E **91**, 043104 (2015)
25. T. Dornheim, T. Schoof, S. Groth, A. Filinov, M. Bonitz, J. Chem. Phys. **143**, 204101 (2015)
26. T. Dornheim, S. Groth, A. Filinov, M. Bonitz, New J. Phys. **17**, 073017 (2015)
27. T. Dornheim, A. Filinov, M. Bonitz, Phys. Rev. B **91**, 054503 (2015)
28. T. Dornheim, S. Groth, T. Schoof, C. Hann, M. Bonitz, Phys. Rev. B **93**, 205134 (2016)
29. K.N. Dzhumagulova, R.U. Masheyeva, T. Ott, P. Hartmann, T.S. Ramazanov, M. Bonitz, Z. Donkó, Phys. Rev. E **93**, 063209 (2016)
30. T. Ott, Z. Donkó, M. Bonitz, Contrib. Plasma Phys. **56**, 246 (2016)
31. S. Groth, T. Schoof, T. Dornheim, M. Bonitz, Phys. Rev. B. **93**, 085102 (2016)
32. T. Dornheim, H. Thomsen, P. Ludwig, A. Filinov, M. Bonitz, Contrib. Plasma Phys. **56**, 371 (2016)
33. T. Dornheim, S. Groth, T. Sjostrom, F.D. Malone, W.M.C. Foulkes, M. Bonitz, Phys. Rev. Lett. **117**, 156403 (2016)
34. T. Dornheim, S. Groth, F.D. Malone, T. Schoof, T. Sjostrom, W.M.C. Foulkes, M. Bonitz, Phys. Plasmas **24**, 056303 (2017)
35. S. Groth, T. Dornheim, M. Bonitz, Contrib. Plasma Phys. **57**, 137 (2017)
36. S. Groth, T. Dornheim, T. Sjostrom, F.D. Malone, W.M.C. Foulkes, M. Bonitz, Phys. Rev. Lett. **119**, 135001 (2017)
37. T. Ott, M. Bonitz, P. Hartmann, Z. Donkó, Phys. Rev. E **95**, 013209 (2017)
38. T. Dornheim, S. Groth, J. Vorberger, M. Bonitz, Phys. Rev. E **96**, 023203 (2017)
39. S. Groth, T. Dornheim, M. Bonitz, J. Chem. Phys. **147**, 164108 (2017)
40. T. Dornheim, S. Groth, M. Bonitz, Contrib. Plasma Phys. **57**, 468 (2017)
41. Z.A. Moldabekov, S. Groth, T. Dornheim, M. Bonitz, T.S. Ramazanov, Contrib. Plasma Phys. **57**, 532 (2017)
42. M.H. Thoma, J. Phys. G **31**, L7 (2005)
43. M.H. Thoma, J. Phys. G **31**, 539 (2005)
44. D.R. Neilson, B.I. Halperin, Phys. Rev. B **19**, 2457 (1979)
45. B.I. Halperin, D.R. Neilson, Phys. Rev. Lett. **41**, 121 (1978)
46. A.P. Young, Phys. Rev. B **19**, 1855 (1979)
47. G.D. Mahan, *Many particle physics* (Kluwer, New York, 2000)
48. P.-F. Loos, P.M.W. Gill, Comput. Mol. Sci. **6**, 410 (2016)
49. S. Ichimaru, Rev. Mod. Phys. **54**, 1017 (1982)
50. S. Ichimaru, H. Iyetomi, S. Tanaka, Phys. Rep. **149**, 91 (1987)
51. M. Bonitz, P. Ludwig, H. Baumgartner, C. Henning, A. Filinov, D. Block, O. Arp, A. Piel, S. Käding, Y. Ivanov, A. Melzer, H. Fehske, V. Filinov, Phys. Plasmas **15**, 055704 (2008)
52. F. Graziani, M.P. Desjarlais, R. Redmer, S.B. Trickey, *Frontiers and challenges in warm dense matter*, Lecture notes in computational science and engineering (Springer International Publishing, Cham, Switzerland, 2014)
53. V.V. Karasiev, T. Sjostrom, J. Dufty, S.B. Trickey, Phys. Rev. Lett. **112**, 076403 (2014)
54. F.D. Malone, N.S. Blunt, E.W. Brown, D.K.K. Lee, J.S. Spencer, W.M.C. Foulkes, J.J. Shepherd, Phys. Rev. Lett. **117**, 115701 (2016)
55. F.D. Malone, N.S. Blunt, J.J. Shepherd, D.K.K. Lee, J.S. Spencer, W.M.C. Foulkes, J. Chem. Phys. **143**, 044116 (2015)
56. S. Tanaka, Contrib. Plasma Phys. **57**, 126 (2017)
57. V.S. Filinov, V.E. Fortov, M. Bonitz, Z. Moldabekov, Phys. Rev. E **91**, 033108 (2015)
58. T. Sjostrom, J. Dufty, Phys. Rev. B **88**, 115123 (2013)
59. S. Dutta, J. Dufty, Phys. Rev. E **87**, 032102 (2013)
60. S. Dutta, J. Dufty, Europhys. **102**, 67005 (2013)
61. E.W. Brown, B.K. Clark, J.L. DuBois, D.M. Ceperley, Phys. Rev. Lett. **110**, 146405 (2013)
62. Y. Liu, J. Wu, J. Chem. Phys. **141**, 064115 (2014)
63. P. Arora, K. Kumar, R.K. Moudgil, Eur. Phys. J. B **90**, 76 (2017)
64. T. Dornheim, S. Groth, M. Bonitz, arXiv:1801.05783 (2018)
65. M. Bonitz, in *Quantum kinetic theory*, 2nd edn. (Springer, Berlin, Germany, 2016)
66. K. Balzer, S. Bauch, M. Bonitz, Phys. Rev. A **82**, 033427 (2010)
67. N. Schlünzen, M. Bonitz, Contrib. Plasma Phys. **56**, 5 (2016)
68. K. Balzer, N. Schlünzen, M. Bonitz, Phys. Rev. B **94**, 245118 (2016)
69. F.H. Zong, C. Lin, D.M. Ceperley, Phys. Rev. E **66**, 036703 (2002)
70. H. Kählert et al., Eur. Phys. J. D **72**, 83 (2018)
71. D. Kremp, M. Schlanges, W.D. Kraeft, *Quantum statistics of nonideal plasmas* (Springer, Berlin, Heidelberg, 2005)
72. A. Filinov, M. Bonitz, Y. Lozovik, Phys. Rev. Lett. **86**, 3851 (2001)
73. J.P. Hansen, I.R. McDonald, *Theory of simple liquids* (Academic Press, London, 2006)
74. G.J. Kalman, K.I. Golden, Z. Donkó, P. Hartmann, J. Phys.: Conf. Ser. **11**, 254 (2005)
75. S. Hamaguchi, R.T. Farouki, D.H.E. Dubin, Phys. Rev. E **56**, 4671 (1997)
76. T. Ott, M. Stanley, M. Bonitz, Phys. Plasmas **18**, 063701 (2011)
77. J. Böning, A. Filinov, P. Ludwig, H. Baumgartner, M. Bonitz, Y.E. Lozovik, Phys. Rev. Lett. **100**, 113401 (2008)
78. V. Golubnychiy, H. Baumgartner, M. Bonitz, A. Filinov, H. Fehske, J. Phys. A **39**, 4527 (2006)

79. K. Balzer, M. Bonitz, R. van Leeuwen, N.E. Dahlen, A. Stan, Phys. Rev. B **79**, 245306 (2009)
80. V.M. Bedanov, F.M. Peeters, Phys. Rev. B **49**, 2667 (1994)
81. A.V. Filinov, Y.E. Lozovik, M. Bonitz, Phys. Status Solidi B **221**, 231 (2000)
82. S.W.S. Apolinario, F.M. Peeters, Phys. Rev. E **76**, 031107 (2007)
83. J. Harting, O. Mülken, P. Borrmann, Phys. Rev. B **62**, 10207 (2000)
84. L.P. Kouwenhoven, D.G. Austing, S. Tarucha, Rep. Prog. Phys. **64**, 701 (2001)
85. S.M. Reimann, M. Manninen, Rev. Mod. Phys. **74**, 1283 (2002)
86. A. Ghosal, A.D. Güclü, C.J. Umrigar, D. Ullmo, H.U. Baranger, Phys. Rev. B **76**, 085341 (2007)
87. A. Ghosal, A.D. Gl, C.J. Umrigar, D. Ullmo, H.U. Baranger, Nat. Phys. **2**, 336 (2006)
88. B. Liu, J. Goree, Y. Feng, Phys. Rev. E **78**, 046403 (2008)
89. L.-J. Hou, A. Piel, P.K. Shukla, Phys. Rev. Lett. **102**, 085002 (2009)
90. T. Ott, M. Bonitz, Z. Donkó, P. Hartmann, Phys. Rev. E **78**, 026409 (2008)
91. T. Ott, M. Bonitz, Phys. Rev. Lett. **103**, 195001 (2009)
92. T. Ott, M. Bonitz, Contrib. Plasma Phys. **49**, 760 (2009)
93. T. Ott, M. Bonitz, Phys. Rev. Lett. **107**, 135003 (2011)
94. S.I. Braginskii, Rev. Plasma Phys. **1**, 205 (1965)
95. Y. Feng, J. Goree, B. Liu, T.P. Intrator, M.S. Murillo, Phys. Rev. E **90**, 013105 (2014)
96. L. Spitzer Jr., Phys. Fluids **3**, 659 (1960)
97. T. Ott, M. Bonitz, P. Hartmann, Z. Donkó, Phys. Rev. E **83**, 046403 (2011)
98. T. Ott, H. Kählert, A. Reynolds, M. Bonitz, Phys. Rev. Lett. **108**, 255002 (2012)
99. D. Page, U. Geppert, M. Küker, Astrophys. Space Sci. **308**, 403 (2007)
100. Z. Donkó, B. Nyíri, L. Szalai, S. Holló, Phys. Rev. Lett. **81**, 1622 (1998)
101. G. Salin, J.-M. Caillol, Phys. Rev. Lett. **88**, 065002 (2002)
102. R. Balescu, in *Transport processes in plasmas*, Classical transport (North-Holland Publishing Company, Amsterdam, 1988), Vol. 1
103. R.T. Delves, Rep. Prog. Phys. **28**, 249 (1965)
104. B. Liu, J. Goree, Phys. Rev. Lett. **94**, 185002 (2005)
105. S. Giorgini, L.P. Pitaevskii, S. Stringari, Rev. Mod. Phys. **80**, 1215 (2008)
106. F. Dalfovo, S. Giorgini, L.P. Pitaevskii, S. Stringari, Rev. Mod. Phys. **71**, 463 (1999)
107. I. Bloch, Nat. Phys. **1**, 23 (2005)
108. V.A. Schweigert, F.M. Peeters, Phys. Rev. B **51**, 7700 (1995)
109. M. Bonitz, K. Balzer, R. van Leeuwen, Phys. Rev. B **76**, 045341 (2007)
110. C. Henning, K. Fujioka, P. Ludwig, A. Piel, A. Melzer, M. Bonitz, Phys. Rev. Lett. **101**, 045002 (2008)
111. J. Neuhaus-Steinmetz, S.I. Mistakidis, P. Schmelcher, Phys. Rev. A **95**, 053610 (2017)
112. G.M. Koutentakis, S.I. Mistakidis, P. Schmelcher, Phys. Rev. A **95**, 013617 (2017)
113. R. Schmitz, S. Krönke, L. Cao, P. Schmelcher, Phys. Rev. A **88**, 043601 (2013)